*Journal of The Electrochemical Society*, **166** (2) F53-F58 (2019)
0013-4651/2019/166(2)/F53/6/$37.00 © The Electrochemical Society


# Processing Nano-YSZ in Solid Oxide Fuel Cells: The Effect of Sintering Atmosphere on Thermochemical Stability

**S. P. Muhoza,[1] A. McCormack,[2] R. W. Garrett,[2] M. D. Yuce,[1] V. S. Prathab,[1] S. K. Hambright,[1] M. A. Cottam,[1] and M. D. Gross [2,3,z]**

[1]*Department of Chemistry, Wake Forest University, Winston-Salem, North Carolina 27109, USA*
[2]*Department of Engineering, Wake Forest University, Winston-Salem, North Carolina 27101, USA*
[3]*Center for Functional Materials, Wake Forest University, Winston-Salem, North Carolina 27109, USA*

The thermochemical stability of nanoscale yttria-stabilized-zirconia (nYSZ), processed via in situ carbon templating, was studied between 850°C–1350°C in four sintering atmospheres: Ar, $N_2$, $H_2$, and humidified $H_2$. The in situ carbon templating method generates nanoscale ceramic particles surrounded by an amorphous carbon template upon sintering. The carbon template is subsequently removed by low temperature oxidation, leaving behind nanoscale ceramic particles. In Ar and $H_2$, a ZrC impurity formed at temperatures ≥1150°C. In humidified $H_2$, either a ZrC impurity formed or the carbon template oxidized. In $N_2$, ZrC was not observed over the temperature range studied and the carbon template was preserved. After carbon template removal, the nYSZ surface areas were high for Ar, $H_2$, and $N_2$: 55–99 $m^2 \cdot g^{-1}$. For humidified $H_2$, nYSZ surface area decreased as the carbon template was lost. Finally, nYSZ, processed in $N_2$ at 850°C and 1250°C, was integrated into symmetric YSZ-Lanthanum Strontium Ferrite (YSZ-LSF) cathode cells. The addition of nYSZ decreased cathode non-ohmic resistance, at 550°C in air, by 40% and 27% for nYSZ processed at 850°C and 1250°C, respectively. This work demonstrates that $N_2$ is a thermochemically stable atmosphere for in situ carbon templating and that the resulting nYSZ considerably improves electrode performance.
 [DOI: 10.1149/2.0261902jes]

Manuscript submitted December 12, 2018; revised manuscript received December 26, 2018. Published January 9, 2019.

We recently developed a processing method that produces high surface area mixed-metal-oxides (up to 99 $m^2 \cdot g^{-1}$) in the 850°C–1350°C temperature range.[1–4] The processing method is referred to as the in situ carbon templating method and has been shown to work for numerous ceramics used in solid oxide fuel cell (SOFC) electrodes, including yttria-stabilized zirconia (YSZ), gadolinia-doped ceria (GDC), lanthanum-strontium-cobalt-iron-oxide (LSCF), and strontium titanate (STO). The in situ carbon templating method involves two steps. First, a hybrid inorganic-organic material, containing the stoichiometric metal salts of the desired mixed-metal-oxide, is sintered between 850°C–1350°C in an inert atmosphere. During sintering, nanoscale mixed-metal-oxide particles and amorphous carbon form. The amorphous carbon surrounds the ceramic nanoparticles, preventing them from sintering into larger particles. In the second step, the amorphous carbon is burned away at 700°C in air, a temperature low enough to preserve the ceramic nanoparticles. We have shown that the processing method works for two hybrid materials: (1) propylene oxide gels with a glucose additive to vary the carbon template concentration[1–4] and (2) citric acid gels; the carbon template concentration is controlled by the concentration of citric acid.[3,4] We have also shown that the surface area of nano-YSZ prepared with this approach is still high after 2000 hours at 500°C (65 $m^2 \cdot g^{-1}$) and 700°C (35 $m^2 \cdot g^{-1}$).[4]

In our early work, the inert processing atmosphere was flowing argon. In the case of YSZ, a small ZrC impurity peak formed upon sintering at 1150°C and at 1350°C ZrC was the primary phase. In most cases, a pure YSZ phase was obtained upon oxidation of the carbon template at 700°C in air; however, a monoclinic $ZrO_2$ impurity phase was detected in some cases.[1] This is a concern because monoclinic $ZrO_2$ is deleterious to the oxygen ion conductivity and electrochemical activity of the SOFC electrodes.[5,6] It has been suggested that the monoclinic $ZrO_2$ phase is most likely the result of limited Zr diffusion from isolated $ZrO_2$ crystallites into the YSZ phase at 700°C. This is supported by the fact that we have observed the monoclinic $ZrO_2$ phase disappear upon oxidation at 900°C. Unfortunately, the YSZ surface area significantly decreased upon heating to 900°C, defeating the purpose of producing high surface area ceramic particles. Another challenge with the presence of ZrC in the electrode composite is that the transformation from ZrC to YSZ corresponds to a dimensional expansion of 17 vol%. Such an expansion may cause the fuel cell to fracture, depending on the composition and electrode composite design.[7–9]

[z]E-mail: grossmd@wfu.edu

Given the challenges associated with the presence of ZrC in the electrode composite, we explored two alternative sintering atmospheres, $N_2$ and humidified $H_2$, to avoid forming ZrC in the first place. Numerous reports have shown that nitrogen dissolves into $ZrO_2$ and partially stabilized YSZ (3 mol% $Y_2O_3$) when sintered in a $N_2$ atmosphere.[10–13] Nitrification occurs near the surface at a low concentration, N/Zr ratio < 0.2, which causes the formation of oxygen vacancies and stabilizes the tetragonal phase. Importantly, neither an oxynitride phase nor a monoclinic $ZrO_2$ formed. In addition, Scheffler et al. reported that a Si-based composite forms a carbide phase in a $N_2$ atmosphere at 1390°C, compared to forming the carbide phase at 1000°C in argon, due to the favorable reactivity of nitrogen with silica.[14] Given these findings, we investigated the effect of sintering YSZ hybrid inorganic-organic materials in $N_2$. The hypothesis was that a ZrC impurity phase would form at a higher temperature in $N_2$ compared to argon.

Humidified $H_2$ was the second sintering atmosphere investigated in this work, which was chosen for two reasons. First, the literature suggests that an oxygen fugacity range should exist, in the 850°C–1350°C temperature range, within which a YSZ-C mixture will be thermochemically stable.[15–17] Above the oxygen fugacity range the carbon would oxidize and below the oxygen fugacity range ZrC would form. The specific fugacity range is not listed here because it changes by orders of magnitude with temperature. Second, oxygen fugacity is easily controlled by varying the level of humidity in $H_2$.

This paper reports on the thermochemical stability, carbon template concentration, and resulting surface area of processing YSZ hybrid materials in Ar, $N_2$, $H_2$, and humidified $H_2$. In addition, the effect of infiltrating nYSZ into symmetric YSZ-Lanthanum Strontium Ferrite (YSZ-LSF) cathode cells was assessed by comparing electrochemical impedance spectra for symmetric cells with and without nYSZ.

## Experimental

YSZ-Propylene Oxide-Glucose (YSZ-POG) hybrid materials were prepared following the same procedure that was used in our previously reported works.[1–4] Briefly, stoichiometric amounts of $ZrCl_4$ (99.5+%, Alfa Aesar), $Y(NO_3)_3 \cdot 6H_2O$ (99.9%, Alfa Aesar), and glucose (≥ 99.9%, Alfa Aesar) were sequentially dissolved in deionized water and magnetically stirred until complete dissolution. Propylene Oxide (PO, ≥ 99.5%, Sigma-Aldrich) was then added to the solution and stirred for about five minutes, after which a translucent yellow gel formed. The gel was aged for 24 h, washed with ethanol (200 Proof, Deacon Lab) once per day for three days, and then dried in an open

container under ambient conditions. The dried gel was ground into a powder and pressed into ∼0.6 g cylindrical pellets with a ∼13 mm diameter and ∼2 mm thickness, by applying a 22 kN force for 90 seconds as detailed in our previous work.[2]

YSZ-POG green pellets were sintered in Ar, $N_2$, $H_2$, and four compositions of humidified $H_2$ (0.01%, 0.03%, 0.3%, and 2.3% $H_2O$). The 97.7% $H_2$/2.3% $H_2O$ gas mixture was created by flowing $H_2$ (99.995%, Airgas) through a water bubbler at room temperature. The lower concentrations of $H_2O$ were created with a Kofloc GASCON GM-2B gas mixer. One inlet port was connected to $H_2$ and the other inlet port was connected to $H_2$ flowing through a bubbler at room temperature or 0°C. The flow rate of each gas stream was adjusted to obtain the desired humidity levels. The total flow rate for the outgoing humidified $H_2$ was held constant at 750 mL/min. The other sintering atmospheres (Ar, $H_2$, and $N_2$) were also flowed over the sample at 750 mL/min. During sintering, the temperature was increased from ambient temperature to 850°C at a rate of 5°C/min, then from 850°C to the sintering temperature at a rate of 2°C/min, held at the sintering temperature for 2 h, decreased to 850°C at a rate of 2°C/min, and then to ambient temperature at a rate of 5°C/min. The sintering temperatures investigated were 850°C–1350°C in 100°C increments. After sintering, the sintered pellets were calcined in air at 700°C to burn off the carbon template.

Powder X-ray diffraction (PXRD) patterns were collected for both the sintered and calcined samples for phase identification. The patterns were collected with a Bruker D2 Phaser X-ray diffractometer with CuKα radiation over a 2θ range of 20°–65° in 0.03° increments and a 0.3 s time step. Thermogravimetric analysis (TGA) was conducted with a TA Instruments SDT Q600 on sintered materials for carbon template concentration determination as described in our previous work.[1] The temperature was ramped from ambient to 1200°C at a rate of 10°C/min in air flowing at 100 mL/min. The Brunauer, Emmett, Teller (BET) method was used to determine the specific surface areas of the calcined materials using a Micromeritics Tristar II 3020 surface area analyzer and $N_2$ as the adsorbate. All samples were degassed under flowing $N_2$ at 250°C for 2 h prior to testing. The surface area values reported in this work had a correlation coefficient of at least 0.9995.

Symmetric YSZ-LSF cathode cells were fabricated by infiltrating LSF into porous YSZ scaffold films that were sintered on both sides of a YSZ electrolyte. The porous YSZ scaffold-dense YSZ electrolyte-porous YSZ scaffold tri-layer was fabricated by laminating three tape-casted films as described elsewhere.[18] The laminated tri-layer was sintered by heating in air to 1500°C at a rate of 2°C/min, holding at 1500°C for 4 h, and then cooling to room temperature at a rate of 2°C/min. Upon sintering, the respective diameters of the electrolyte and electrode layers were 15.0 mm and 7.7 mm and the respective thicknesses were 100 μm and 50 μm. The porous YSZ layers were infiltrated with YSZ-POG solution, prior to gelation, and then sintered to 850°C or 1250°C in $N_2$ for 2 h followed by calcination in air at 700°C for 2 h. At this point, the porous YSZ scaffolds had been decorated with YSZ nanoparticles at a loading of ∼2.5 vol% of the electrode. The modified YSZ scaffolds were then infiltrated with an LSF aqueous solution composed of $La(NO_3)_3{\cdot}6H_2O$ (99.99%, Alfa Aesar), $Sr(NO_3)_2$ (99.0%, Alfa Aesar), $Fe(NO_3)_3{\cdot}9H_2O$ (98+%, Alfa Aesar), and citric acid (CA, 99.8%, US Biological) dissolved in water with a La:Sr:Fe:CA molar ratio of 0.8:0.2:1:2. The cells were heated to 400°C in air for 10 min after each of the first three infiltrations and then to 850°C for 30 min after the fourth infiltration. This process was repeated until a LSF loading of 25 vol% of the electrode was achieved. For comparison, YSZ-LSF symmetric cells without YSZ nanoparticles were also prepared.

Electrochemical impedance spectra were collected for the symmetric cells using a Gamry Instruments Series G750 potentiostat with four probes. The electrodes were painted with silver ink for current collection and silver wires were used to connect the electrodes to the potentiostat. Impedance spectra were collected in the galvanostatic mode with a 0 mA dc current, 5 mA ac perturbation, and $10^{-1}$–$10^6$ Hz frequency range. All cells were tested at 550°C in air, the ohmic contributions were subtracted from the impedance, and the non-ohmic impedance values were multiplied by 0.5 to normalize the contribution of the two identical electrodes. Porous scaffolds with and without YSZ nanoparticles were imaged with scanning electron microscopy (SEM) with a FEI Verios 460L FESEM (Hillsboro, OR) electron microscope.

## Results and Discussion

PXRD patterns of YSZ-POG sintered in flowing Ar, $H_2$, and $N_2$ are presented in Figure 1. In each case, patterns of both the sintered and calcined materials are shown. After sintering YSZ-POG in Ar, a ZrC phase formed at 1150°C and its relative peak intensity increased with increasing temperature. Upon calcination in air at 700°C, the material reverts to pure YSZ for all samples, Figure 1a. These results are consistent with our previously reported works in which YSZ-POG was sintered under Ar.[1–4] Figure 1b shows PXRD patterns of YSZ-POG sintered in $H_2$. Similar to the results with Ar, a ZrC phase formed starting at 1150°C and its peak intensity increased with increasing temperature. Additional small impurity peaks were observed after sintering at 1250°C and 1350°C, Figure 1c. The peaks at 1350°C were identified to be monoclinic $Y_2O_3$ and, based on the work of Sulaiman et al., the impurity peaks at 1250°C are likely a mixture of zirconium oxides.[19] Most importantly, however, pure YSZ phases were obtained upon calcination in air at 700°C for all samples. Figure 1d shows PXRD patterns of YSZ-POG sintered in $N_2$. Unlike sintering in Ar and $H_2$, no ZrC phase was observed below 1350°C. Only small ZrC peaks were observed at 1350°C, indicating that sintering in $N_2$ successfully mitigated ZrC formation.

The YSZ peaks in Figure 1 were broad for all samples calcined in air, indicating high surface area. For the samples sintered in Ar and $N_2$, prior to calcination in air, the YSZ peaks were extremely broad at all sintering temperatures. The samples sintered in $H_2$, however, showed a different peak width behavior as sintering temperature was increased. The YSZ peaks were extremely broad at 850°C and 950°C, began to narrow at 1050°C, further narrowed at 1150°C, then broadened at 1250°C, and at 1350°C YSZ peaks were not detectable. To provide a more quantitative comparison of this behavior, YSZ crystallite sizes of the sintered samples, estimated using the Scherrer equation, are shown in Figure 2. In agreement with the consistently large YSZ peak widths for samples sintered in Ar and $N_2$, crystallite size consistently fell within a 2 nm-5 nm range for all sintering temperatures. The crystallite size for samples sintered in $H_2$ spiked to 16 nm at 1150°C and then decreased to 9 nm at 1250°C. To explain the changes in crystallite size, TGA experiments were conducted on sintered samples in the presence of flowing air to quantify the concentration of YSZ, carbon, and ZrC in each sample.

Table I shows vol% concentrations of YSZ, carbon template, and ZrC for samples sintered in Ar, $N_2$, and $H_2$. The YSZ vol% consistently fell in the 15 vol%-19 vol% range for all sintering temperatures under Ar and $N_2$. For the samples sintered in $H_2$, however, the YSZ concentration increased to 28 vol% at 1050°C and reached a maximum of 37 vol% at 1150°C. Correspondingly, the concentration of carbon template decreased at these temperatures, which most likely occurred due to a reaction between $H_2$ and carbon, forming small hydrocarbons.[20] The observed increase in YSZ concentration corresponded to an increase in the crystallite size; the maximum crystallite size of 16 Å at 1150°C occurred at the maximum YSZ concentration of 37 vol%. A similar relationship between YSZ concentration and crystallite size has been previously reported.[2] Additionally, samples sintered in $H_2$ resulted in high concentrations of ZrC upon sintering at 1250°C and 1350°C unlike those sintered in Ar and $N_2$. To form the ZrC phase, Zr diffuses out of the YSZ lattice, which increases the $Y_2O_3$:$ZrO_2$ mol% ratio in the YSZ phase. At 1350°C, we calculated this ratio to be 55:45 which is above the solubility threshold of $Y_2O_3$ in $ZrO_2$ (40:60).[21] This is most likely why $Y_2O_3$ impurity peaks were observed for samples sintered at 1350°C in $H_2$ (Figures 1b–1c).

As shown in Table II, however, surface areas of samples calcined in air at 700°C after being sintered in $H_2$ (50 $m^2$/g–75 $m^2$/g) were

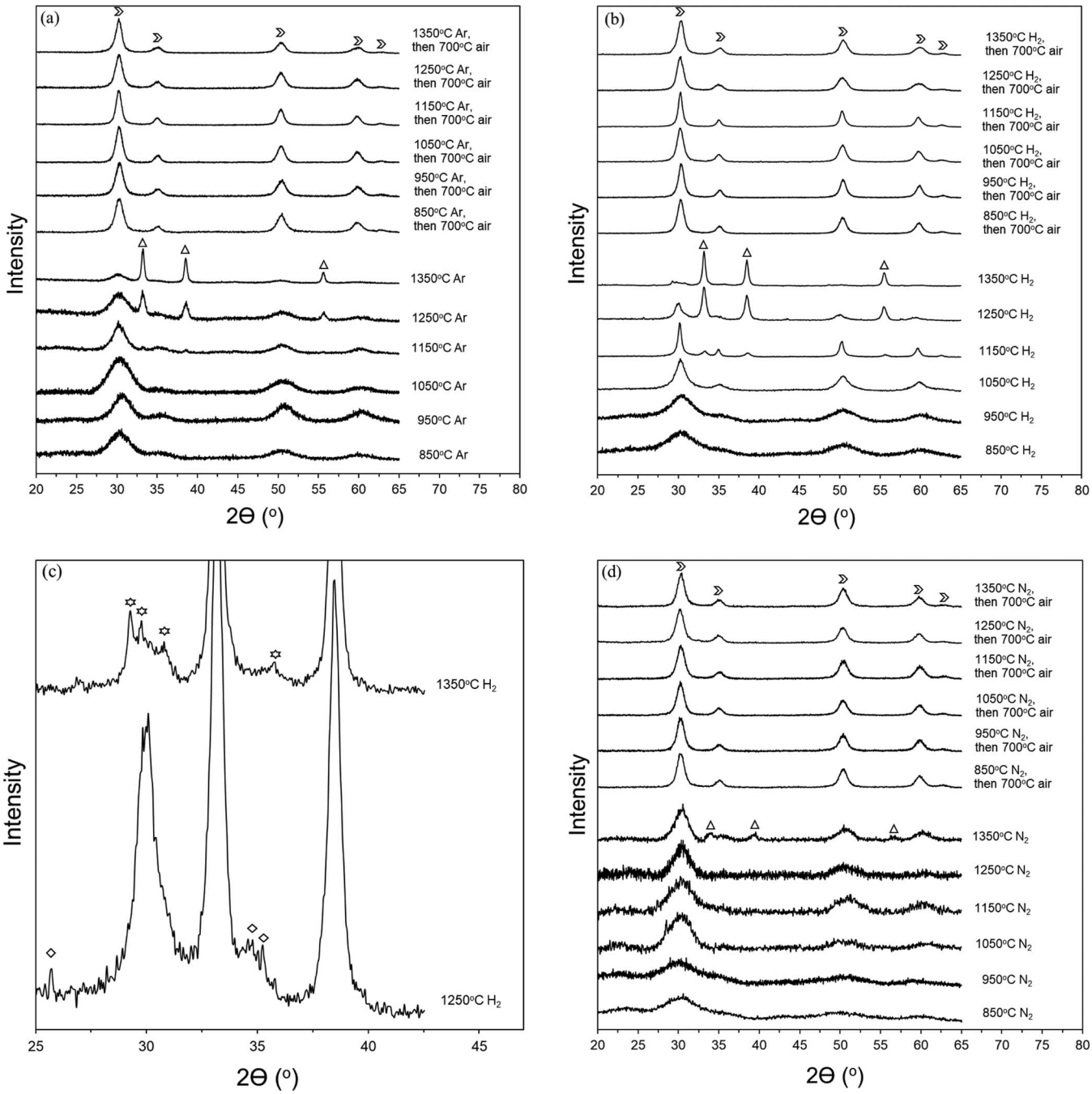


**Figure 1.** Powder X-ray diffraction patterns of YSZ-POG sintered at 850°C–1350°C for 2 h in a) argon, b) and c) hydrogen, and d) nitrogen. The zoomed in view of b) is shown in c). YSZ (≫), ZrC (△), $Y_2O_3$ (✡), and $ZrO_x$ (◇) phases were observed.

comparable to those obtained with Ar (55 $m^2$/g–70 $m^2$/g) and $N_2$ (58 $m^2$/g – 100 $m^2$/g). This suggests that the reduction of carbon template concentration, diffusion of Zr out of YSZ upon sintering in $H_2$, and the diffusion of Zr back into YSZ upon calcination in air did not have a significant impact on the surface area of the final material.

Although sintering in $H_2$ did not have a significant impact on the final surface area of YSZ, a large concentration of ZrC formed during sintering, which is a concern because there is a 17 vol% expansion that occurs upon oxidation of ZrC to $ZrO_2$. Thus, we investigated the thermochemical stability of YSZ-POG sintered in various concentrations of humidified $H_2$ at 1050°C–1350°C using PXRD. For simplicity, only the 1250°C PXRD patterns are shown in Figure 3. The PXRD patterns at other temperatures were similar, either showing a ZrC impurity phase or a pure YSZ phase. The four concentrations of humidified $H_2$ studied were 0.01%, 0.03%, 0.3%, and 2.3% $H_2O$ with the balance being $H_2$. The levels of humidification were chosen based on the theoretical stability of YSZ-C mixtures as a function of oxygen fugacity, Figure 4a. The theoretical thermochemical stability map has three zones. In the bottom zone, the low oxygen fugacity region, carbon will react with Zr to form ZrC. Since there is an excess of carbon in our system relative to Zr (Table I), all of the Zr should react to ZrC, leaving behind excess carbon and $Y_2O_3$. Hence, three phases ($Y_2O_3$, ZrC, and Carbon) should coexist in this zone. The oxygen fugacities in the middle zone should be high enough to prevent the formation of

**Table I. Vol% composition of YSZ-POG sintered at 850°C–1350°C in Ar, $N_2$, and $H_2$.**

| | Ar | | | $N_2$ | | | $H_2$ | | |
|---|---|---|---|---|---|---|---|---|---|
| | ZrC | Carbon Template | YSZ | ZrC | Carbon Template | YSZ | ZrC | Carbon Template | YSZ or (YSZ + $Y_2O_3$)* |
| 850°C | 0 | 85 | 15 | 0 | 84 | 16 | 0 | 81 | 19 |
| 950°C | 0 | 83 | 17 | 0 | 83 | 17 | 0 | 80 | 20 |
| 1050°C | 0 | 83 | 18 | 0 | 83 | 17 | 0 | 72 | 28 |
| 1150°C | 0 | 81 | 19 | 0 | 84 | 16 | 4 | 60 | 37 |
| 1250°C | 2 | 81 | 17 | 0 | 83 | 17 | 15 | 67 | 18 |
| 1350°C | 4 | 79 | 17 | 0.2 | 83 | 17 | 38 | 51 | 12* |

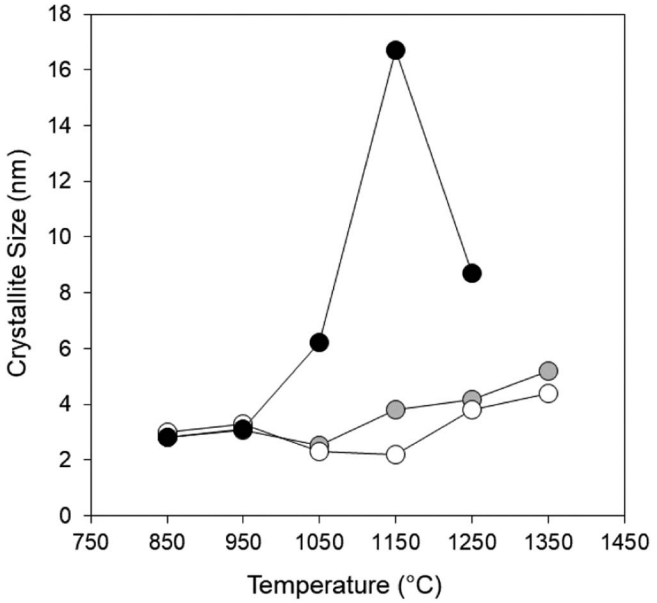


**Figure 2.** YSZ crystallite sizes of YSZ-POG samples sintered at 850°C–1350°C for 2 h in hydrogen (●), argon (◍), and nitrogen (○).

ZrC, but too low to oxidize the carbon template. Thus, only 2 phases (YSZ and Carbon) should be present in this zone, which is the result we were trying to achieve with humidified $H_2$. In the upper zone, carbon should completely oxidize, leaving only one phase (YSZ). The lower boundary of the thermochemical stability map was calculated based on a study by A. Maitre and P. Lefort on the solid-state reaction between $ZrO_2$ and carbon[17] while the upper boundary was calculated based on an oxides Ellingham diagram.[16] As shown in Figure 4a, the $H_2/H_2O$ mixtures we studied should, theoretically, result in a stable YSZ-C mixture or an oxidation of the carbon template, leaving behind YSZ. Theoretically, none of the $H_2/H_2O$ mixtures should have resulted in the formation of ZrC.

Figure 4b maps the experimental thermochemical stability of sintered YSZ-POG based on a combination of PXRD results (Figure 3) and TGA results (Table III). Experimentally, we found two possible results with sintering in humidified $H_2$; either a ZrC impurity formed or a mixture of YSZ and a diminished concentration of carbon template formed. At 1050°C and 1150°C, no ZrC formed for all four levels of humidification. At 1250°C, ZrC formed for 0.01% $H_2O$/99.99% $H_2$ and at 1350°C, ZrC formed at 0.01% $H_2O$/99.99% $H_2$ and 0.03% $H_2O$/99.97% $H_2$. As shown in Table III, TGA results indicate that the concentration of carbon template decreased with an increase in humidity concentration at 1250°C. All carbon template concentrations were lower than the pure $H_2$ result shown in Table I. While not shown here for simplicity, similar trends were observed at all sintering temperatures. The presence of a reduced concentration of carbon template rather than complete oxidation is most likely a result of slow kinetics and not representative of equilibrium. The resulting surface areas of samples sintered in humidified $H_2$ followed by calcination in air at 700°C are also shown in Table III. The surface area of the sample sintered in 0.01% $H_2O$/99.99% $H_2$ was the same as the sample sintered in pure $H_2$. This is not surprising considering the concentration of ZrC formed in both samples was similar. As the concentration of water vapor increased, both the carbon template concentration and surface area decreased. A similar trend between carbon template concentration and surface area has been previously reported.[1–4]

The purpose of this work was to investigate the thermochemical stability of sintering YSZ-POG in various sintering atmospheres with the goal of finding conditions that would allow one to create a stable mixture of YSZ and carbon template, resulting in pure nYSZ upon

**Table II. Specific surface areas in $m^2/g$ of YSZ-POG sintered at 850°C–1350°C in Ar, $N_2$, and $H_2$ and subsequently calcined at 700°C in air.**

| | Ar | $N_2$ | $H_2$ |
|---|---|---|---|
| 850°C | 55 | 58 | 57 |
| 950°C | 65 | 59 | 51 |
| 1050°C | 70 | 60 | 64 |
| 1150°C | 63 | 66 | 74 |
| 1250°C | 61 | 83 | 72 |
| 1350°C | 67 | 99 | 72 |

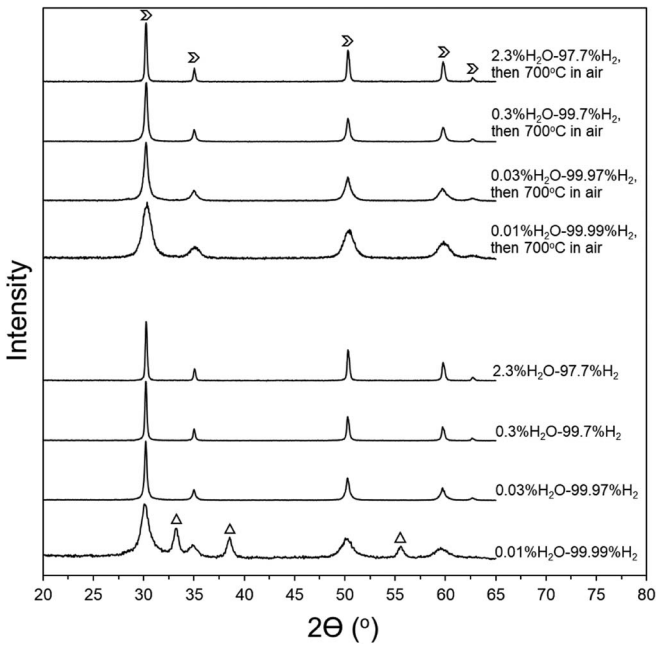


**Figure 3.** Powder X-ray diffraction patterns of YSZ-POG sintered at 1250°C for 2 h in humidified hydrogen at different water vapor concentrations. YSZ (≫) and ZrC (△) phases were observed.

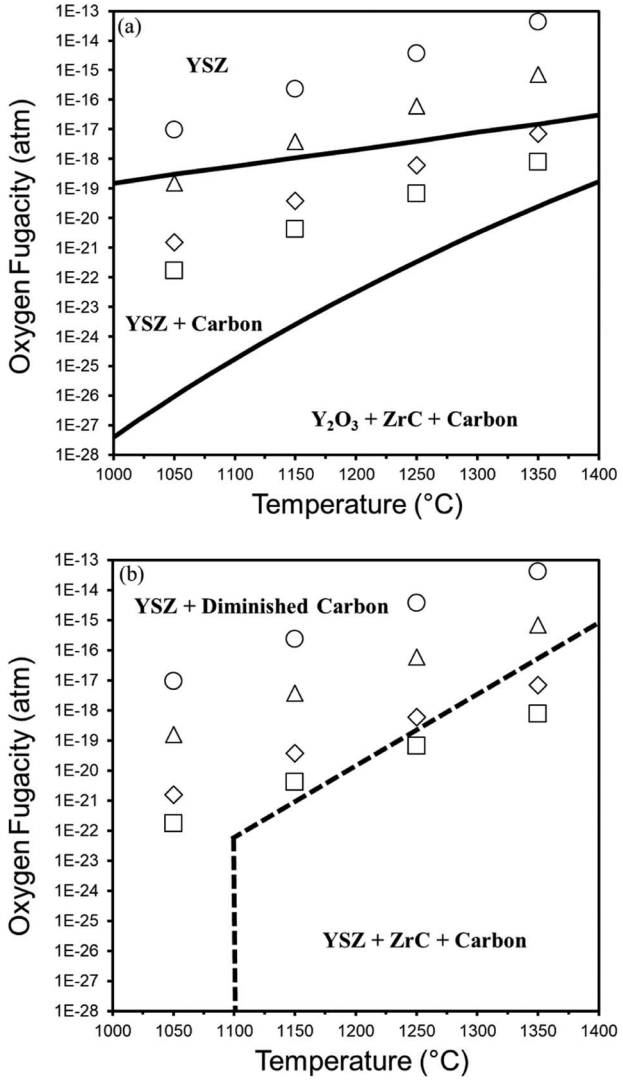


**Figure 4.** a) Estimated theoretical thermochemical stability of YSZ/C system as a function of oxygen fugacity and temperature. b) Experimental observations for YSZ-POG sintered under humidified hydrogen at various water vapor concentrations. 0.01%$H_2O$ – 99.99%$H_2$ (□), 0.03%$H_2O$ – 99.97%$H_2$ (◇), 0.3%$H_2O$ – 99.7%$H_2$ (△), and 2.3%$H_2O$ – 97.7%$H_2$ (○).

calcination in air at 700°C. Among Ar, $N_2$, $H_2$, and various levels of humidified $H_2$, $N_2$ was the most effective sintering atmosphere as it mitigated ZrC formation without affecting the carbon template and surface area. For this reason, we continued with the rest of the study using a $N_2$ sintering atmosphere.

With a thermochemically stable sintering environment established, we investigated the effect of adding nYSZ to the electrochemical impedance of symmetric YSZ-LSF cathode cells. YSZ-POG was

**Table III. Vol% composition of YSZ-POG sintered at 1250°C in humidified $H_2$ as a function of water vapor concentration and surface area of the powders obtained upon subsequent calcination at 700°C in air also as a function of water vapor concentration.**

| | % Water Vapor in the $H_2O/H_2$ Mixture | | | |
|---|---|---|---|---|
| | 0.01% | 0.03% | 0.30% | 2.30% |
| YSZ (vol%) | 38 | 67 | 87 | 96 |
| ZrC (vol%) | 9 | 0 | 0 | 0 |
| Free Carbon (vol%) | 53 | 33 | 13 | 4 |
| Surface Area ($m^2/g$) | 72 | 64 | 47 | 5 |

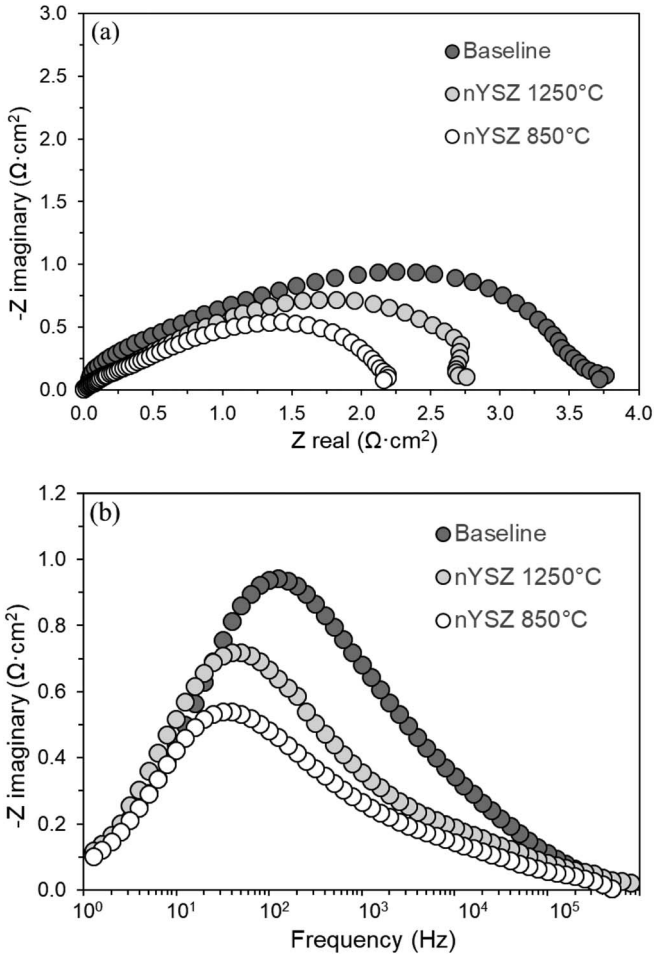


**Figure 5.** a) Nyquist and b) Bode plots of YSZ-LSF symmetrical cells tested at 550°C. The baseline cell contained no YSZ nanoparticles (●) while the other cells were integrated with YSZ nanoparticles via infiltration of YSZ-POG into electrode scaffolds, followed by sintering in $N_2$ at 1250°C (◎) and 850°C (○), and subsequently calcined in air at 700°C.

infiltrated into porous YSZ electrode scaffolds, heated in a $N_2$ atmosphere, then calcined in air. Subsequently, LSF was infiltrated into the scaffold. Figure 5a shows the electrochemical impedance spectra of symmetric cells with and without nYSZ at 550°C in air. The non-ohmic resistance of the cell without nYSZ was 3.75 $\Omega \cdot cm^2$. The addition of nYSZ processed at 850°C in $N_2$ reduced the non-ohmic resistance to 2.2 $\Omega \cdot cm^2$, a 40% reduction in non-ohmic resistance. This value is equivalent to what we have previously reported for symmetric cells fabricated using Ar.[3,4] In that work, nYSZ improved the impedance up to an operating temperature of 700°C; above 700°C the impedance with and without nYSZ was indistinguishable. The addition of nYSZ processed at 1250°C in $N_2$ reduced the non-ohmic resistance to 2.75 $\Omega \cdot cm^2$, a 27% reduction compared to the cell without nYSZ. The corresponding Bode plots are shown in Figure 5b. The maximum in the Bode plot decreases from the baseline cell without nYSZ to the cell with nYSZ processed at 1250°C to the cell with nYSZ processed at 850°C. The frequency at which the maximum occurs also decreases from 125 Hz to 60 Hz to 40 Hz for the baseline, 1250°C, and 850°C cells, respectively. Characteristic frequencies in the 10 Hz-150 Hz range have been shown to correspond to cathode activation polarization.[22–25] Thus, the addition of nYSZ to YSZ-LSF cathodes decreased cathode activation polarization. More specifically, other groups have suggested that the observed improvement may be due to diffusivity of oxygen ions through the LSF bulk as well as migration and incorporation of oxygen ions from the three-phase boundary (TPB) into the YSZ electrolyte lattice.[23–25] One could

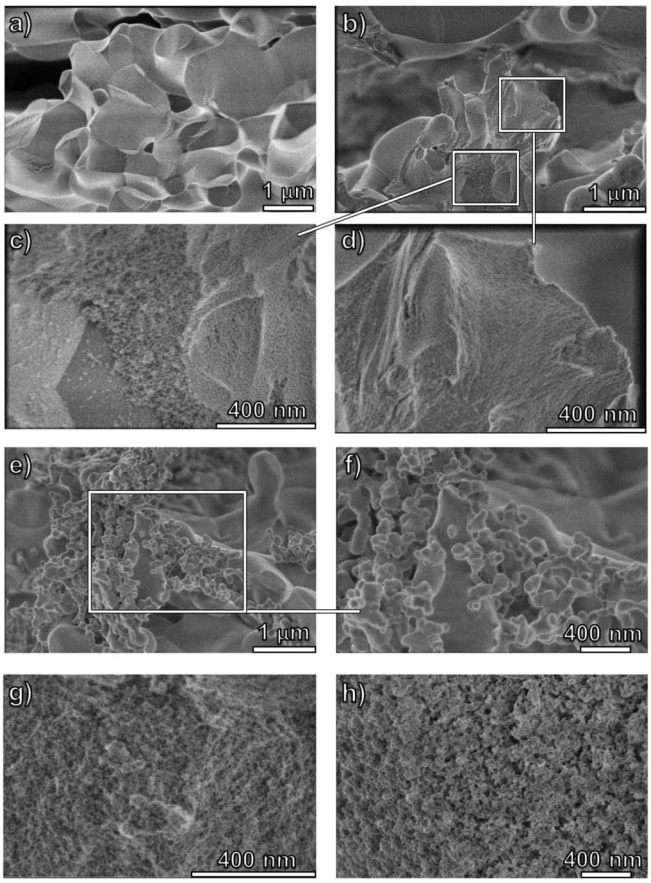


**Figure 6.** SEM images of YSZ-LSF electrode scaffolds without nYSZ (a) and with nYSZ processed at 850°C (b-d) and 1250°C (e-f) in $N_2$, followed by calcination at 700°C in air. SEM images of nYSZ powder obtained upon sintering YSZ-POG pellets at 850°C (g) and 1250°C (h) in $N_2$ and subsequently calcining at 700°C in air are also shown on the figure.

argue that the addition of nYSZ increases the density of TPB and/or shortens the diffusion length of oxygen ions to the YSZ scaffold. It is interesting that the peak frequency in the Bode plot decreases with decreasing impedance; typically peak frequency increases with decreasing impedance. We suspect the observed trend may be due to the morphology of the nano-YSZ layer between the low surface area traditional YSZ scaffold and the infiltrated LSF phase and is an area for future study.

SEM was used to explore the morphology of nYSZ on the surface of the YSZ scaffolds. Figure 6 shows SEM images of the baseline YSZ electrode scaffold (Figure 6a), scaffold with nYSZ processed in $N_2$ at 850°C (Figures 6b–6d), and scaffold with nYSZ processed in $N_2$ at 1250°C (Figures 6e–6f). For comparison, SEM images of nYSZ powder processed in $N_2$ at 850°C and 1250°C are shown in Figures 6g and 6h, respectively. In Figure 6c, the nYSZ processed at 850°C is of order $10^1$ nm. While one can see texture on the surface of the YSZ scaffold in Figure 6d, it is difficult to estimate a particle size from this image. The surface area of the nYSZ sample processed at 850°C and represented in both Table II and Figure 6g was 58 $m^2 \cdot g^{-1}$. Assuming the nYSZ particles were spherical and of uniform size, the particle diameter would be 17 nm. Thus, the morphology of the nYSZ generated from a pressed pellet of YSZ-POG and generated in a porous YSZ scaffold are similar. At 1250°C, however, the morphology of the nYSZ generated from a pressed pellet of YSZ-POG and generated in a porous YSZ scaffold are quite different. As shown in Figure 6f, the nYSZ particle size is of order $10^2$ nm. This particle size is significantly larger than the nYSZ shown in Figure 6h. We suggest the larger nYSZ particles in the YSZ scaffold may be due to loss of carbon template. Carbon, which is a reducing environment, could have pulled oxygen from the YSZ scaffold, resulting in the oxidation of some fraction of the carbon template. As we have shown, surface area is directly proportional to carbon template concentration and, thus, particle size and carbon template are inversely proportional. We are currently investigating this possibility. Nevertheless, the addition of nYSZ processed at both 850°C and 1250°C significantly reduced the cathode impedance, demonstrating that this is a promising approach to improving cathode performance.

## Conclusions

Various sintering atmospheres were studied to mitigate carbide formation, a critical limitation to the in situ carbon templating method. The best outcomes were obtained under $N_2$. First, sintering in $N_2$ did not form ZrC at $\leq$ 1250°C while only a small amount of ZrC was observed at 1350°C. Second, the highest carbon template concentrations and surface areas were obtained with $N_2$. Finally, the electrochemical performance of symmetric YSZ-LSF cathode cells was improved by up to 40% at 550°C in air via addition of YSZ nanoparticles processed under $N_2$.

## Acknowledgments

This work was supported by the National Science Foundation Faculty Early Career Development (CAREER) award (CMMI-1651186). We also thank Charles Mooney and Dr. Cynthia Day for their assistance with SEM and XRD data collection, respectively.

## ORCID

M. D. Gross https://orcid.org/0000-0002-2280-2034

## References

1. M. Cottam, S. Muhoza, and M. D. Gross, *J. Am. Ceram. Soc.*, **99**, 2625 (2016).
2. S. P. Muhoza, M. A. Cottam, and M. D. Gross, *J. Vis. Exp.*, **122**, e55500 (2017).
3. S. P. Muhoza, T. E. Barrett, S. E. Soll, and M. D. Gross, *ECS Trans.*, **78**, 1407 (2017).
4. S. P. Muhoza, T. E. Barrett, M. A. Cottam, S. E. Soll, M. D. Yuce, V. S. Prathab, S. K. Hambright, M. Rezazad, O. Racchi, and M. D. Gross, *J. Electrochem. Soc.*, **165**, F46 (2018).
5. K. Apriany, I. Permadani, D. G. Syarif, S. Soepriyanto, and F. Rahmawati, *IOP Conf. Ser.: Mater. Sci. Eng.*, **107**, 12023 (2016).
6. D. Eder and R. Kramer, *Phys. Chem. Chem. Phys.*, **8**, 4476 (2006).
7. Q. Fu, F. Tietz, D. Sebold, S. Tao, and J. T. S. Irvine, *J. Power Sources*, **171**, 663 (2007).
8. A. N. Busawon, D. Sarantaridis, and A. Atkinson, *Electrochem. Solid State Lett.*, **11**(10), B186 (2008).
9. B. H. Smith and M. D. Gross, *Electrochem. Solid State Lett.*, **14**(1), B1 (2011).
10. T. J. Chung, H. Song, G. H. Kim, and D. Y. Kim, *J. Am. Ceram. Soc.*, **80**(10), 2607 (1997).
11. Y. K. Paek, J. H. Ahn, G. H. Kim, and S. J. L. Kang, *J. Am. Ceram. Soc.*, **85**(6), 1631 (2002).
12. A. Diaz-Parralejo, A. L. Ortiz, F. Rodriguez-Rojas, and F. Guiberteau, *Thin Solid Films*, **518**, 2779 (2010).
13. M. Lerch, *J. Am. Ceram. Soc.*, **79**(10), 2641 (1996).
14. M. Scheffer, E. Pippel, J. Woltersdorf, and P. Greil, *Mater. Chem. Phys.*, **80**, 565 (2003).
15. S. R. Shatynski, *Oxid. Met.*, **13**(2), 105 (1979).
16. A. Maitre and P. Lefort, *Solid State Ion.*, **104**, 109 (1997).
17. D. R. Gaskell, *Introduction to the Thermodynamics of Materials*, (4th Ed.), p. 429, Taylor & Francis, New York (2003).
18. M. D. Gross, J. M. Vohs, and R. J. Gorte, *J. Electrochem. Soc.*, **154**, B694 (2007).
19. S. N. Basahel, T. T. Ali, M. Mokhtar, and K. Narasimharao, *Nanoscale Res. Lett.*, **10**, 73 (2015).
20. L. A. Calderon, E. Chamorro, and J. F. Espinal, *Carbon*, **118**, 597 (2017).
21. V. S. Stubican, R. C. Hink, and S. P. Ray, *J. Electrochem. Soc.*, **61**, 18 (1978).
22. S. Lee, N. Miller, and K. Gerdes, *J. Electrochem. Soc.*, **159**(7), F301 (2012).
23. A. Leonide, V. Sonn, A. Weber, and E. Ivers-Tiffee, *J. Electrochem. Soc.*, **155**(1), B36 (2008).
24. X. J. Chen, K. A. Khor, and S. H. Chan, *J. Power Sources*, **123**, 17 (2003).
25. A. Leonide, B. Ruger, A. Weber, W. A. Meulenberg, and E. Ivers-Tiffee, *J. Electrochem. Soc.*, **157**(2), B234 (2010).